Available online at www.sciencedirect.com
SCIENCE DIRECT
Polymer 47 (2006) 1036–1043
polymer
www.elsevier.com/locate/polymer

Temperature dependent variations in the lamellar structure of poly(L-lactide)

Tai-Yon Cho *, Gert Strobl

Physikalisches Institut, Albert-Ludwigs-Universität Freiburg, Hermann-Herder-Str. 3, 79104 Freiburg, Baden-Wurttemberg, Germany

Received 23 November 2005; accepted 9 December 2005

Abstract

Time- and temperature-dependent SAXS and WAXS experiments on poly(L-lactide) were used (i) to establish the relationships between the crystallization temperature, the crystal thickness and the melting point, (ii) to follow recrystallization processes during heating, and (iii) to detect perturbations of the crystalline order. The studies showed several peculiarities: (i) although no solid state thickening occurs during a crystallization, crystal thicknesses are with values between 11 and 20 nm very large (ii) crystal thicknesses and long spacings have a minimum at 120 °C and increase for both higher and lower crystallization temperatures. The anomalous behavior at low crystallization temperatures is to be related with a disordering of the crystal lattice (iii) there exists an extended temperature range where crystal thicknesses change in controlled manner by recrystallization processes (iv) as it appears, a triple point where the fluid, the crystalline and a mesomorphic phase coexist is located near to normal pressure and a temperature of 190 °C.

Keywords: Polymer crystallization; Poly(L-lactide); Small angle X-ray scattering

1. Introduction

Poly(L-lactide) (PLLA) is a biodegradable semi-crystalline polymer widely investigated in view of biomedical applications and possible uses as a compostable commodity material. Degradation can be achieved by chemical or enzymatic hydrolysis (compare [1] and the references cited therein). The structure of the crystals forming from the melt was first determined by De Santis and Kovacs [2] as being set-up of left-handed 10_3-helices packed in quasi-hexagonal manner into an orthorhombic unit cell. Later, more detailed works including analysis by vibrational spectroscopy pointed at slight distortions of the basic helical conformation due to interchain forces [3,4]. Being semi-crystal, the mechanical properties of PLLA depend on the details of the crystalline–amorphous structure, which vary as always with the crystallization conditions. An overview about crystallinities and crystal thicknesses after crystallizations from the melt for both PLLA and related statistical copolymers was provided by Runt and coworkers [5–7]. It shows that the crystallinity is high, more than 50%, and crystal thickesses as well as long spacings are large, usually above 10 and 20 nm, respectively.

Time- and temperature-dependent SAXS experiments carried out during the last years for various crystallizing polymers-polyethylene, *i*- and *s*-polypropylene, poly(ε-caprolactone)[8], poly(1-butene)[9], *i*-polystyrene [10]—showed us that the relationships between crystallization temperature, crystal thickness and melting points can be exactly established and provide insights into the mechanism of polymer crystallization. The results contradicted basic assumptions of conventional views and led us to a novel model [11]. We now carried out analogous SAXS experiments for PLLA, and obtained again unexpected results. In particular, the thickness of the crystals developing at low temperatures near to T_g is with 13 nm much higher than for all cold crystallized systems investigated so far. We relate this to a peculiarity in the crystallization behavior of PLLA: crystals remain imperfect, when they grow at low temperatures [12].

2. Experimental section

2.1. Samples

Experiments were carried out on samples of a poly(L-lactide) produced by Sigma-Aldrich. The molar mass was $M_w = 101.000$ ($M_w/M_n = 1.7$).

* Corresponding author. Address: School of Chemistry, Seoul National University, Seoul, South Korea.
E-mail address: tai-yon@physik.uni-freiburg.de (T.-Y. Cho).

0032-3861/$ - see front matter © 2005 Elsevier Ltd. All rights reserved.
doi:10.1016/j.polymer.2005.12.027

2.2. Simultaneous small and wide angle X-ray scattering

Small angle and wide angle X-ray scattering experiments were conducted simultaneously with the aid of a twin camera produced by Hecus and Braun, Graz, Austria. In this device a Kratky small angle camera is complemented by a second camera which registers the X-ray scattering in the angular range $2\theta = 19-26°$ (θ: Bragg scattering angle). Small angle and wide angle X-ray scattering curves are registered separately, employing two one-dimensional position-sensitive wire detectors. The intensity data obtained are stored and further evaluated in a PC. We used a Cu anode, fabricated by Bruker AXS, Karlsruhe, Germany, as X-ray source, together with a Ni-filter to extract the K_α radiation.

2.2.1. Evaluation of SAXS data

Having determined the primary beam intensity with the aid of a moving slit system, desmeared scattering curves were obtained in absolute values, as differential cross sections per unit volume $\Sigma(q)$. With a knowledge of $\Sigma(q)$, the one-dimensional electron density auto-correlation function $K(z)$ and its second derivative $K''(z)$, which gives the interface distance distribution function [13,14], can be directly calculated by applying the Fourier relations

$$K(z) = \frac{1}{r_e^2}\frac{1}{(2\pi)^3}\int_0^\infty \cos(qz)4\pi q^2\Sigma(q)\mathrm{d}q \tag{1}$$

and

$$K''(z) = \frac{2}{r_e^2(2\pi)^2}\int_0^\infty [\lim_{q\to\infty} q^4\Sigma(q) - q^4\Sigma(q)]\cos(qz)\mathrm{d}q \tag{2}$$

Here, q denotes the scattering vector $q = 4\pi \sin\theta/\lambda$; r_e is the classical electron radius.

2.2.2. WAXS reflection linewidths

Line widths were measured for the 203-Bragg reflection, the strongest reflection in the registered part of the WAXS curve. In order to determine the coherence length, D_{hkl} a Gaussian function

$$I(\Delta\theta) = \frac{1}{\sigma\sqrt{2\pi}}\exp\left(-\frac{(\Delta\theta)^2}{2\sigma^2}\right) \tag{3}$$

was adjusted to the profile of the reflection after its separation from the background ($\Delta\theta = \theta - \theta_{hkl}$). D_{hkl} then followed from the Scherrer equation [15] as

$$D_{hkl} = \frac{\lambda}{2\cos\theta\sqrt{2\pi}\sigma} \tag{4}$$

$\sqrt{2\pi}\sigma$ is the integral width of the reflection.

2.3. Temperature-dependent WAXS and DSC

Additional WAXS curves which extended over a large angular range and their changes during heating were registered in temperature-dependent measurements with a Siemens D500 diffractometer.

DSC experiments were carried out using a Perkin–Elmer DSC-7.

3. Results

We first present here in a few figures a number of characteristic observations known from the literature, since they provide the basis of understanding of the new SAXS experiments. The latter are reported in the second part of this section.

3.1. Characteristic general observations

Figs. 1–3 show a collection of typical images which appear when the crystallization of PLLA is observed in a polarizing

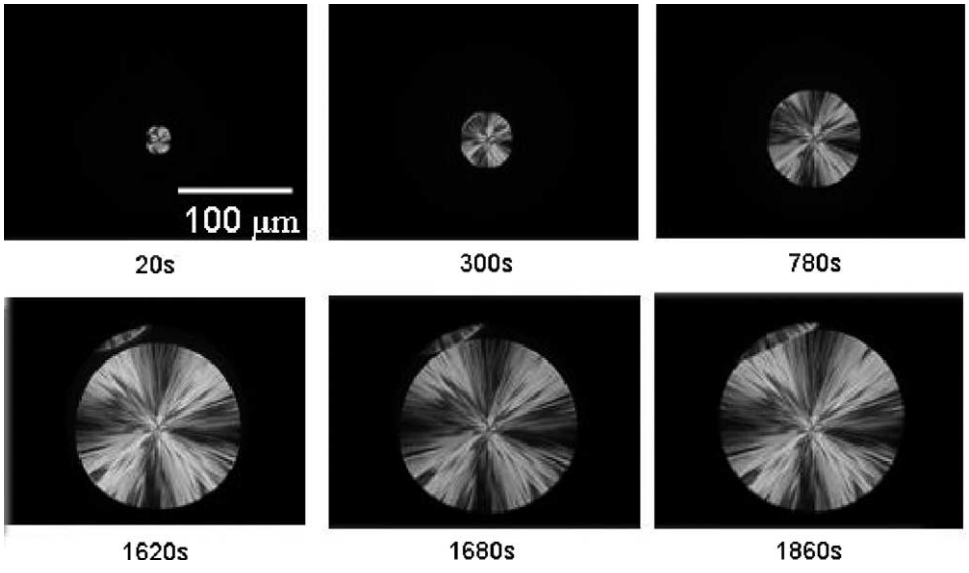

Fig. 1. A spherulite of PLLA growing at 130 °C as observed in a polarizing optical microscope.

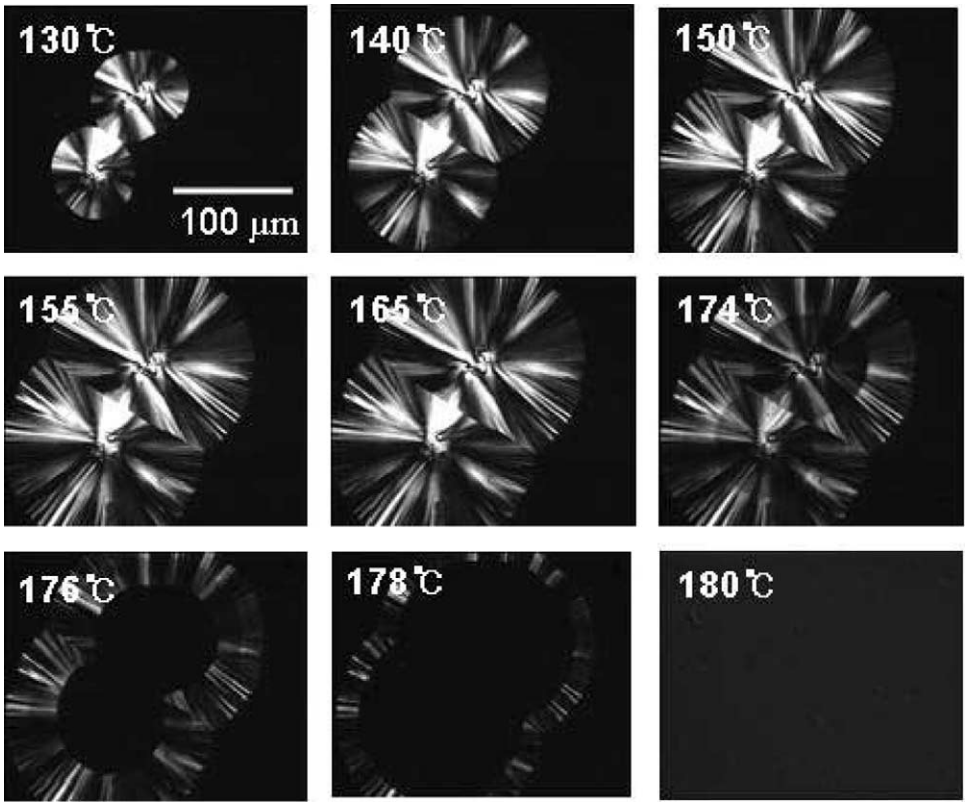

Fig. 2. Observations in a POM when running a temperature program with step-wise temperature rises. The sample was kept for 600 s at each temperature.

optical microscope. At high crystallization temperatures, i.e. temperatures above 130 °C, the number of nuclei is usually very low. One observes as a consequence only a few spherulites which can grow to macroscopic sizes in the order of several 100 μm. Fig. 1 shows as an example the growth of an individual spherulite which takes place with a constant growth rate of typically several microns per minute. The spherulites have a negative birefringence, with the *a*-axis of the orthorhombic unit cell being oriented in radial direction [16]. Crystallization temperatures and melting points are generally related, in the sense that an increase in the crystallization temperature leads also to an increase in the melting point. Fig. 2 demonstrates this dependence for PLLA in a nice manner. During the crystallization process the sample was kept at a sequence of step-like increasing temperatures, at each temperature for a period of 600 s. The crystallization process began with a cooling from the melt to the initial crystallization temperature, $T_c = 130$ °C, and then continued with several temperature steps. The two spherulites shown in the images grow until a temperature of 155 °C is reached, and from thereon keep a constant size; growth rates for the even higher temperatures were obviously too low to be recorded. Of interest are the subsequent melting processes. Melting starts at 174 °C where the first inner part grown at 130 °C disappears. At 176 °C those parts of the spherulite which have grown up to 140 °C also melt, and at 180 °C those which have developed at the highest temperature with crystal growth, 155 °C, vanish.

The appearance completely changes if a low crystallization temperature is chosen, for example $T_c = 82$ °C, as is depicted in Fig. 3. In this case, the sample was at first quenched to the glassy state and then set at the crystallization temperature. The nucleation density is now extremely high; even at the end of the crystallization processes it is impossible to resolve in the microscope individual spherulites. This strong increase in the nucleation density is, however, not the only change taking place at low crystallization temperatures. This becomes apparent in the WAXS patterns, in a comparison of the results of high temperature crystallizations with low temperature

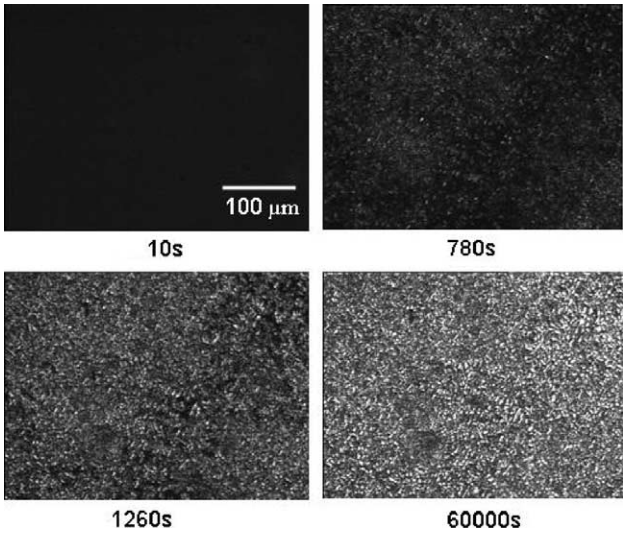

Fig. 3. Structure evolution at 82 °C coming from the glassy state as observed in a POM.

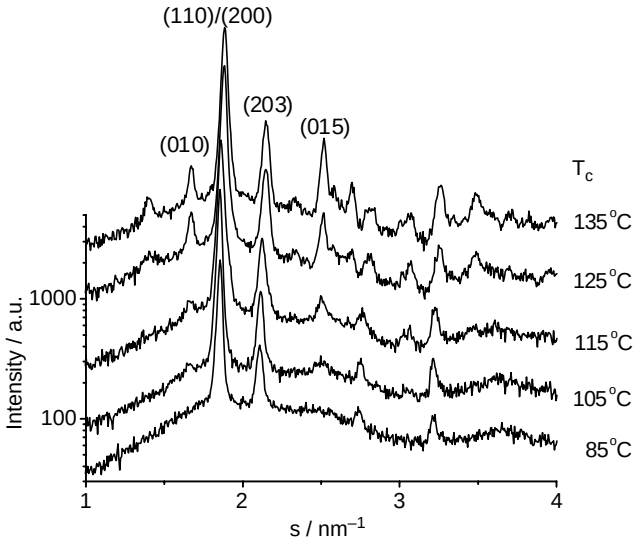

Fig. 4. WAXS curves obtained after isothermal crystallizations at different T_cs indicating a change in the crystalline order. Assignments of the reflections in the ordered orthorhombic phase.

crystallizations [12,17]. Such a series of patterns is depicted in Fig. 4. As is obvious, several of the Bragg reflections which show up at high T_cs disappear when the crystallization is carried out a low temperatures. The pattern measured after a crystallization at 85 °C shows no longer the 015-reflection, and several other reflections have also disappeared. On the other hand, the main reflection with the strongest intensity, which includes contributions of both, the 110- and the 200-reflection of the orthorhombic lattice, still exists. The change in the crystal structure indicated by the modification of the scattering pattern is associated with a decrease in the interchain distance on increasing the crystallization temperature. This change, as derived from the reflection position, is depicted in Fig. 5. The conclusions which can be drawn from the changing WAXS pattern are obvious, and they agree with conclusions to be drawn from corresponding changes of the IR-spectra [12]. While the crystals which form at crystallization temperatures above 130 °C are well ordered, this is no longer the case for the low T_cs. The chains are still packed in quasi-hexagonal manner, however, the rotational and longitudinal ordering is highly perturbed. This relates in particular to the formation of dipole–dipole bridges between the CH_3 and C=0 groups on adjacent chains. Therefore, not only the less dense packing but also the reduction of specific interactions between neighboring chains lead to a decrease in the cohesive energy of the crystal. This decrease shows up in a drop of the heat of fusion, by an amount of 20 J g^{-1} as is shown in Fig. 6.

The decreasing crystalline order shows also up in an anomaly in the temperature dependence of the growth if the spherulites. After a first maximum is passed at around 130 °C, the rate increases again at around 120 °C, then reaching a second, higher maximum around 115 °C [18,19]. Formation of less perfect crystals thus takes place more rapidly, which appears conceivable.

One may ask whether or not full order can be introduced into an initially disordered crystal by an annealing at

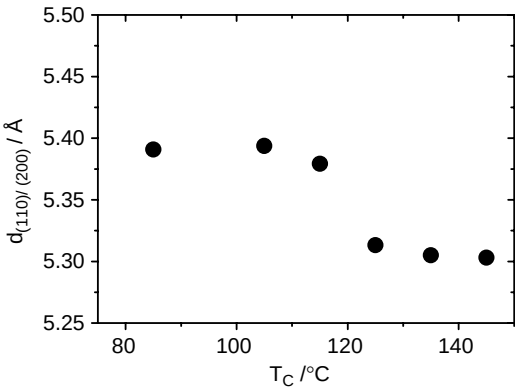

Fig. 5. Temperature dependent spacing of the 110/200 lattice planes as derived from the positions of the reflections in Fig. 4.

temperatures above 130 °C. Fig. 7 shows that this is not the case; higher temperatures are necessary to achieve an ordering. Heating perturbed crystals obtained by a crystallization at 80 °C leads only at temperatures above 155 °C to the appearance of the characteristic 015-reflection. This retarded onset of ordering is also confirmed by the DSC run for the at 80 °C crystallized sample, as depicted in Fig. 8. One finds an exothermal contribution in the heat flow around 160 °C which is to be associated with the formation of perfect crystals [20].

3.2. SAXS experiments: temperature dependent variations in the lamellar structure

At first we employed SAXS experiments in studies of the lamellar structure formed by the perfect crystals which develop at crystallization temperatures above 130 °C. Fig. 9 depicts a typical result, showing the interface distance distribution functions derived from measured SAXS curves during an isothermal crystallization at 143 °C (upper figure) and during a subsequent heating (lower figure). The time dependent part related to the isothermal crystallization indicates a growth of crystals with a thickness d_c=16 nm, amorphous intercrystalline layers with a thickness d_a=6 nm and a long spacing, i.e. a distance between the centers of adjacent crystallites of d_{ac}= 22 nm. No thickening takes place during the crystallization

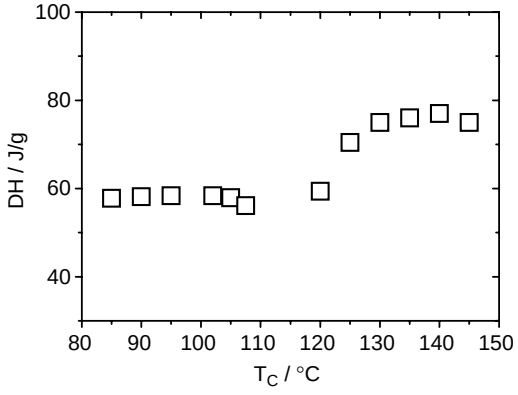

Fig. 6. Heats of fusion determined subsequent to isothermal crystallization processes at different T_cs.

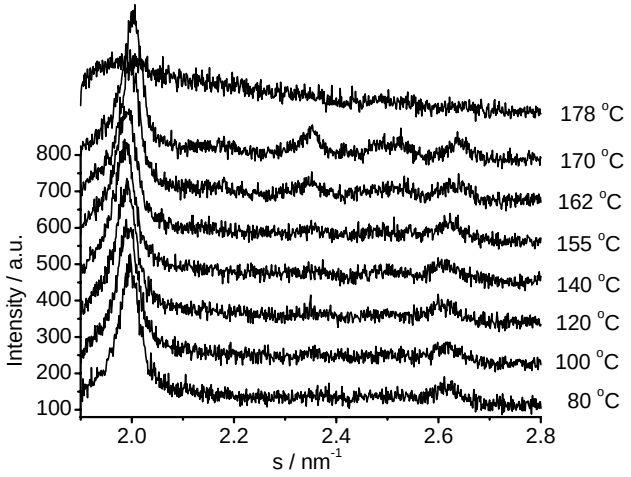

Fig. 7. WAXS patterns measured during the heating of a sample crystallized at 80 °C.

process. The values of d_c and d_{ac} are remarkably large, much larger than the ones found for all other polymer systems investigated so far—polypropylene, poly(ethylene-*co*-octene)s, polystyrene, poly(ε-caprolactone) and poly(1-butene). The crystallinity is also rather high, with a value of the linear crystallinity

$$\phi_l = \frac{d_c}{d_{ac}} = 0.7$$

The value agrees with that given by the heat of fusion

$$\phi_c = \frac{\Delta H}{\Delta H_0} = 0.73$$

choosing $\Delta H_0 = 106\ \mathrm{J\ g^{-1}}$ [21]. The IDFs indicate that this structure remains stable up to a temperature of 162 °C. Then recrystallization processes set in, resulting in an increase in both, the crystal thickness d_c and the long spacing d_{ac}. The temperature 170 °C marks the melting point as announced by a sharp decrease of all amplitudes. At the melting point crystals have reached a thickness of 20 nm, and the long spacing has increased to 28 nm.

Fig. 10 collects all the crystal thickness values obtained in such time- and temperature-dependent experiments, in plots of the inverse thickness, d_c^{-1}, versus the temperature. Experiments

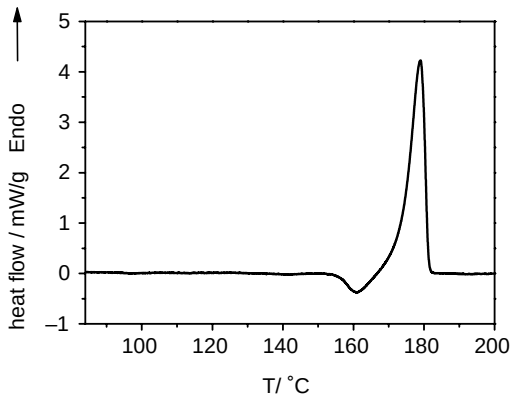

Fig. 8. DSC thermogram measured after an isothermal crystallization at 80 °C.

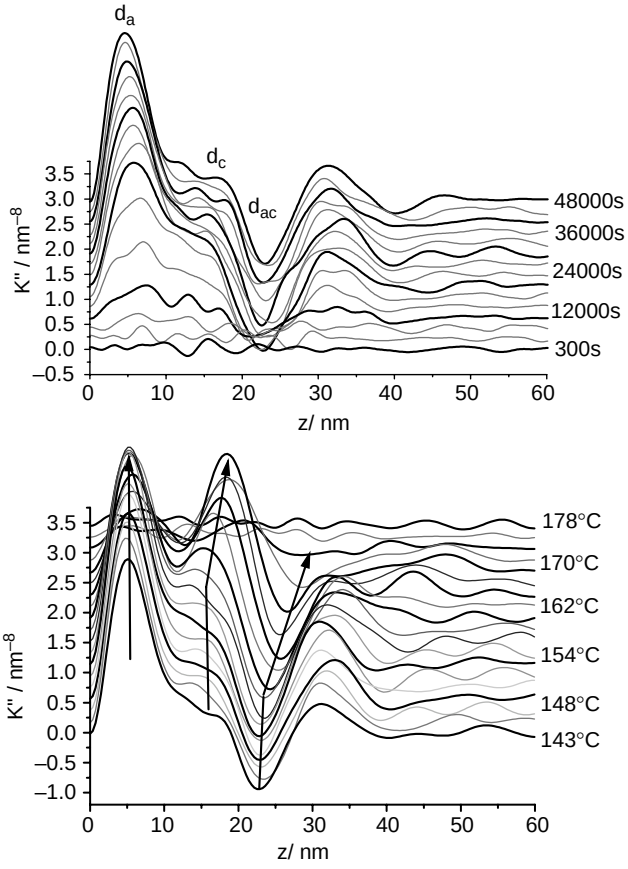

Fig. 9. Isothermal crystallization at 143 °C (top) followed by heating (bottom). IDFs derived from the SAXS curves.

were carried out for temperatures of isothermal crystallization $T_c = 125$, 130, 140 and 143 °C. In addition, the result of a measurement for $T_c = 160$ °C is included. At this highest temperature we used self-seeding to start crystal growth. The initial values measured at the end of the crystallization processes at the different temperatures are all located on a line. As in all the previous works we address it as the 'crystallization line'. The pairs of final values in the heating runs giving the melting point and the associated crystal

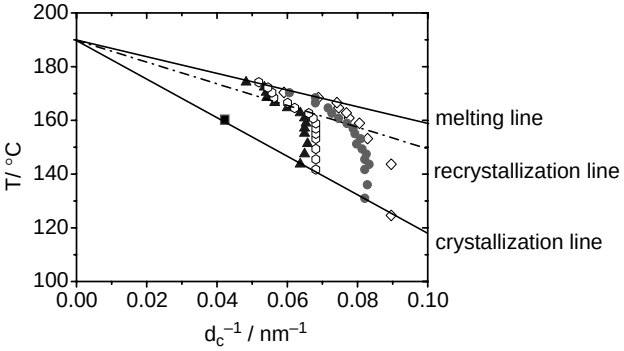

Fig. 10. Results of temperature dependent SAXS experiments: variation of the inverse crystal thickness, d_c^{-1}, during heating runs subsequent to isothermal crystallizations at 125, 130, 140 and 143 °C. The first values in each run are located on the crystallization line, the last values lie on the melting line. The values in the temperature range of recrystallization follow a third line.

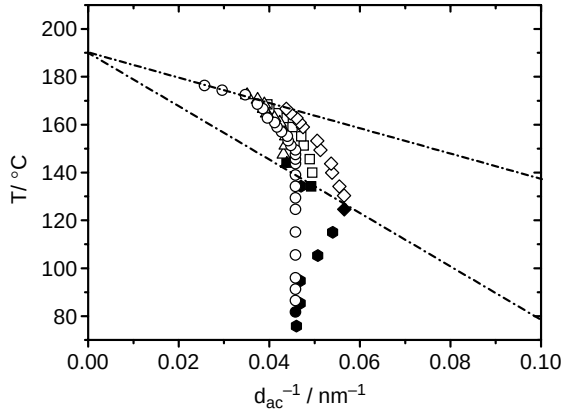

Fig. 11. Filled symbols: inverse long spacings, d_{ac}^{-1}, measured after isothermal crystallizations at different temperatures coming from the melt or the glassy state. Open symbols: variation with temperature of d_{ac}^{-1} during subsequent heating runs.

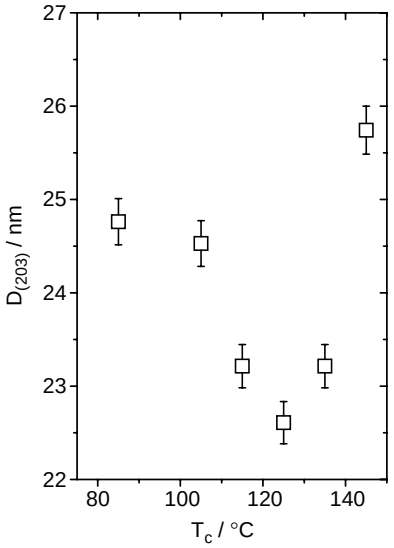

Fig. 12. Correlations lengths D_{203} derived from the linewidth of the 203-reflection after isothermal crystallizations at various temperatures.

thickness establish the Gibbs–Thomson melting line. As an additional feature, experiments point at the existence of a 'recrystallization line'. It determines the onset of recrystallization processes—quite clearly for the series following for $T_c =$ 140 and 143 °C—and then describe also the successive points. As it appears, all three lines, i.e. the crystallization line, the recrystallization line and the melting line commonly extrapolate for $d_c^{-1} \to \infty$, i.e. for macroscopic crystals to a temperature of 190 °C.

All these results refer to the properties of the perfect crystals growing from the melt at temperatures above 130 °C. Quite different results are obtained in the other range, i.e. for crystallization processes at temperatures below 130 °C. These are better reached coming from the glassy state. In fact, it turned out as irrelevant whether the crystallization temperature was reached from the melt or the glassy state, of importance is T_c only. Fig. 11 collects values obtained for the long spacing both for the high and the low temperature range. All the filled points in the figure were measured at the end of isothermal crystallization processes which varied between 75 and 143 °C. Long spacings found in the high temperature region are again located on a line. Those found in the low temperature range no longer follow this line, but deviate towards larger long spacings. As can be seen, the long spacing here increases with decreasing T_c. Such a behavior is peculiar and is found here for the first time. The value observed at the lowest temperature, 75 °C, is with 22 nm unusually large. We are not aware of any system, which would produce such thick lamellar crystallites shortly above the glass transition temperature. Important to note, the coherence length derived from the line width of the 203-reflection changes in equivalent manner. As shown in Fig. 12, D_{203} has a minimum of 125 °C and increases for both higher and lower T_cs. Fig. 11 includes also the results of heating runs, at first once again, subsequent to isothermal crystallizations at T_cs above 130 °C, and then in addition, for the structure formed at 75 °C. The temperature dependent WAXS patterns shown in Fig. 7 indicated that the crystals remain imperfect up to a temperature of 155 °C. The SAXS values of the long spacing show now that d_{ac} remains stable up to a similar temperature. Together or slightly after the perfectioning a total reorganization of the lamellar structure sets in. It leads through the same sequence of reorganized crystal structures as in the case of crystals which have been perfect from the very beginning.

Hence, as long as the temperature remains below 155 °C, no structure changes take place in the cold crystallized sample, either within the crystals as a perfectioning or for the whole structure in the sense of a thickening and long spacing increase. Fig. 13 depicts scattering curves measured in a heating–cooling cycle between 100 and 145 °C. Scattering curves remain invariant in their shape and just change their intensity. The intensity change is obviously due to an increase in the electron density difference between the (imperfect) crystals and the melt only. At low temperatures the density difference virtually vanishes, which prevents a SAXS analysis. It was possible to derive from the SAXS curve measured at the highest temperature, 145 °C, the electron density correlation function

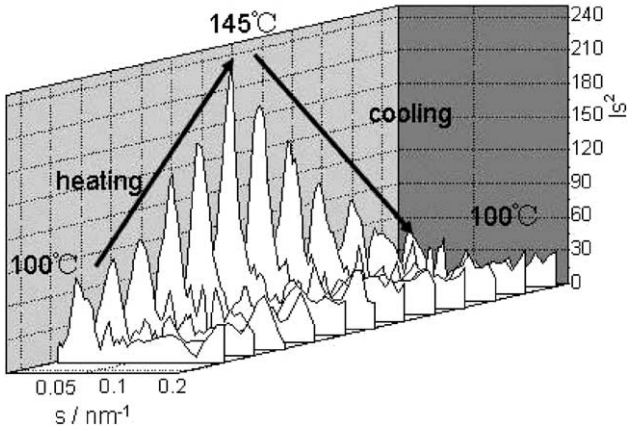

Fig. 13. PLLA, crystallized at 80 °C from the glassy state. SAXS curves measured during a heating–cooling cycle with a maximum temperature of 145 °C.

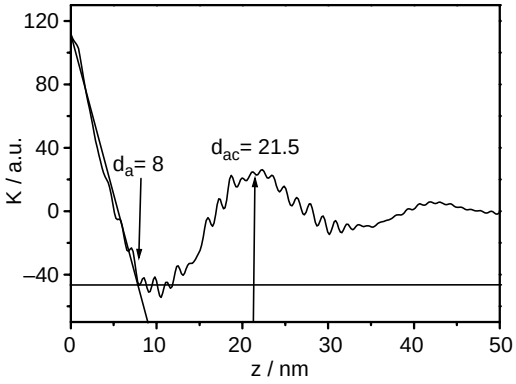

Fig. 14. PLLA, crystallized at 80 °C from the glassy state and heated to 145 °C. Correlation function derived from the SAXS curve.

$K(z)$, and it is presented in Fig. 14. As the result shows, the structure formed at 80 °C is set up of crystallites with a thickness $d_c \simeq 13.5$ nm at a distance of 21.5 nm.

4. Discussion

The Gibbs–Thomson melting line is well determined by the d_c values measured at the various melting points at the end of heating scans after crystallizations at different T_cs. The starting point at $d_c^{-1} = 0$ represents the equilibrium melting point which has the value $T_f^\infty = 190$ °C. For polymers which exhibit an extensive recrystallization before melting, temperature dependent SAXS experiments indeed present the only way for a reliable determination of T_f^∞. The remaining uncertainty is that of the linear extrapolation, which here amounts to some degrees. Interesting to note, the same extrapolated value follows from a plot of melting temperatures versus the inverse long spacings measured at the points of fusion. The corresponding line, shown in Fig. 11, also ends at 190 °C. The strict relation between the two lines is due to an invariance of the linear crystallinity ϕ_l through all temperatures.

As for all other studied crystallizing polymers, we find a linear relationship also between the inverse crystal thickness and the crystallization temperature, with the restriction that this relationship holds here only for the range of higher temperatures, $T_c \geq 130$ °C. Different from the other systems, the crystallization line ends, when linearly extrapolated, at the same temperature as the melting line, i.e. at the equilibrium melting point T_f^∞. Actually, one cannot be sure if this is strictly valid, but the two limiting temperatures certainly are near to each other.

For the low temperature range, $T_c < 130$ °C, crystal thicknesses no longer follow the crystallization line. Indeed, thicknesses and also long spacings here increase when the crystallization temperature is lowered. The lateral coherence length D_{203} shows according to Fig. 12 the same tendency. In our understanding crystal thicknesses are selected by a size dependent phase transition [11]. The entrance step during growth is always the formation of a mesomorphic block with minimum size at the growth front. This block spontaneously expands until that size is reached where the transition into the crystalline phase occurs. In PLLA crystal blocks are very large, always larger than 10^3 nm^3. For sure, blocks of this size cannot form directly by a fluctuation out of the melt. A selection of the crystal thickness by this phase transition implies that the crystallization line extrapolates in the macroscopic limit to the coexistence temperature T_{mc}^∞ between the mesomorphic and the crystalline phase. For PLLA our results would indicate a location of T_{mc}^∞ near to the equilibrium melting point at 190 °C. This, however, would mean that 190 °C not only represents the melting point but is, even more, a triple point where the mesomorphic, the amorphous and the crystalline phase coexist. We do not think that this is strictly true, because a coexistence exactly at normal pressure is highly improbable, but the triple point could well be located close to it, i.e. at a slightly different temperature and a slightly different external pressure.

How would the block sizes change when at lower crystallization temperatures crystals are no longer perfect but show more and more disorder? The sketch in Fig. 15 is meant to give an answer. The dotted line describes the change in the Gibbs free energy per monomer when the mesomorphic block expands at T_c. It forms with a minimum size at point 1 which includes an activation step for the necessary density fluctuation in the melt. At high temperatures, where perfect crystals form, the transition takes place at point 2a where the Gibbs free energies of the mesomorphic layer and perfect crystalline layers (dashed line) coincide. If at lower temperatures only imperfect crystals form, their Gibbs free energy is enhanced with a regard to the perfect crystals. This leads to an upward shift of the associated free energy line (dash–dotted). Coincidence of the free energy with that of the mesomorphic layer is now only reached after a further expansion, at point 2b. The WAXS patterns in Fig. 4 indicate a continuous increase in the disorder of the crystals. Hence, one has to expect a continuous shift of the transition points to larger values of d_c. The largest values are reached at the lowest T_cs, since here the disordering is maximal.

In our model, this first formation of crystalline blocks out of the mesophase is always followed by a stabilization process resulting from some surface reorganization. The existence of such a step becomes apparent in the extended temperature

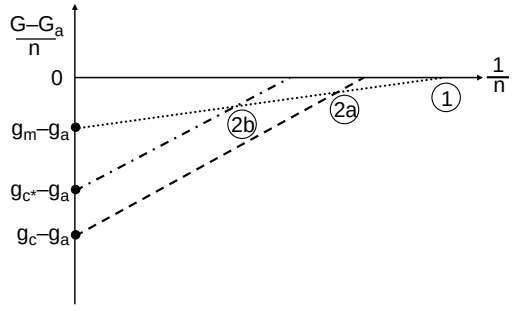

Fig. 15. Gibbs free energies per monomer as a function of the inverse layer thickness (difference to the melt value g_a at some fixed temperature). Lines refer to layers with mesomorphic (dotted), perfect-crystalline (dashed) and perturbed-crystalline (dash–dotted) order. Minimum thickness of the mesomorphic layer (1), points of transition into a perfect (2a) or an imperfect (2b) crystal.

range with a constant block size, which is always found when heating an isothermally crystallized sample. For the perfect crystals this holds up to some temperature which is well defined for $T_c = 140$ and 143 °C. Here, the system enters on heating a range of continuous recrystallization processes. Recrystallization occurs at a nearly constant crystallinity—is therefore barely visible in DSC scans—and it obviously takes place very rapidly establishing at each actual temperature a new thickness. Interesting to note, also in the range of continuous recrystallization one finds a linear dependence between the thickness and the actual temperature, and, as indicated by the results in Fig. 11, this 'recrystallization line' also extrapolates to 190 °C. Since not only the thickness but also the long spacing L changes simultaneously we encounter here a total reorganization of the structure. In our view, it is a short transition step into the mesophase rather than a short melting which enables the system to reorganize so rapidly. In fact, the proposed thermodynamic scheme predicts such a process [11]. A recent work of Fujita and Doi [22] shows the recrystallization of PLLA directly in in situ AFM observations. Temperature steps are accompanied by step-like increases in the thickness of a single crystal. The process is very rapid, and retains the crystal shape, as it is to be expected for a short transition of blocks into a mesophase. Blocks can indeed be seen at the crystal edges after a recrystallization, with a size of about 20 nm as is indicated by the WAXS line width.

For $T_c = 143$ °C, the ongoing recrystallization ends at around 170 °C. Here now, the crystals indeed melt, as is indicated by a simultaneous drop of both the WAXS and SAXS intensities. We have presently no answer to the question about the reason for the ending of the recrystallization at this point.

Also disordered crystallites exhibit an extended stability range. For $T_c = 80$ °C it is going up to 155 °C. The transition into the ordered crystal structure then takes place abruptly rather than continuously. Hence, it is probable that also this transition uses a passage through the mesophase. When the ordered crystal blocks have formed they have the same properties as those which directly developed at high T_cs. A recrystallization sets in at the same temperature.

Hence, our model can explain the observations. Of course, this does not represent a proof, however, gives more support.

Acknowledgements

Support of this work by the Deutsche Forschungsgemeinschaft is gratefully acknowledged. Thanks are also due to the 'Fonds der Chemischen Industrie' for financial help.

References

[1] Kikkawa Y, Abe H, Iwata T, Inoue Y, Doi Y. Biomacromolecules 2002;3:350.
[2] De Santis J, Kovacs P. Biopolymers 1968;6:299.
[3] Aleman C, Lotz B, Puigalli J. Macromolecules 2001;34:4795.
[4] Kang S, Hsu SL, Stidhand HD, Smith PB, Leugers MA, Yang X. Macromolecules 2001;34:4542.
[5] Huang J, Lisowski MS, Runt J, Hall ES, Kean RT, Buehler N, et al. Macromolecules 1998;31:2593.
[6] Baratian S, Hall ES, Lin JS, Xu R, Runt J. Macromolecules 2001;34:4857.
[7] Cho J, Baratian S, Kim J, Yeh F, Hsiao B, Runt J. Polymer 2003;44:711.
[8] Heck B, Hugel T, Iijima M, Sadiku E, Strobl G. New J Phys 1999;1:17.
[9] Fu Q, Heck B, Strobl G, Thomann Y. Macromolecules 2001;34:2502.
[10] Al-Hussein M, Strobl G. Macromolecules 2002;35:8515.
[11] Strobl G. Eur Phys J, E; ER 2005;18:295.
[12] Zhang J, Duan Y, Sato H, Tsuji H, Noda I, Yan S, et al. Macromolecules 2005;38:8012.
[13] Ruland W. Colloid Polym Sci 1977;255:417.
[14] Schmidtke J, Strobl G, Thurn-Albrecht T. Macromolecules 1997;30:5804.
[15] Guinier A. X-ray diffraction: W.H.Freeman. San Francisco; 1963 p. 124.
[16] Kalb B, Pennings AJ. Polymer 1980;21:607.
[17] Ohtani Y, Okumura K, Kawaguchi A. J Macromol Sci Phys 2003;3:875.
[18] Di Lorenzo ML. Eur Polym J 2005;41:569.
[19] Abe H, Kikkawa Y, Inoue Y, Doi Y. Biomacromolecules 2001;2:1007.
[20] Iannace S, Nicolais L. J Appl Polym Sci 1997;64:911.
[21] Sarasua J, Prud'homme RE, Wisniewski M, Le Borgne A, Spassky N. Macromolecules 1998;31:3895.
[22] Fujita M, Doi Y. Biomacromolecules 2003;4:1301.